Measurements of Tropospheric OH Concentrations: A Comparison of Field Data with Model Predictions

D. PERNER*, U. PLATT, M. TRAINER**, G. HÜBLER**, J. DRUMMOND, W. JUNKERMANN, J. RUDOLPH, B. SCHUBERT, A. VOLZ***, and D. H. EHHALT

K. J. RUMPEL

and

G. HELAS

Abstract. Using long path UV absorption spectroscopy we have measured OH concentrations close to the earth's surface. The OH values observed at two locations in Germany during 1980 through 1983 range from 0.7×10^6 to 3.2×10^6 cm^{-3}. Simultaneously we measured the concentrations of O_3, H_2O, NO, NO_2, CH_4, CO, and the light non methane hydrocarbons. We also determined the photolysis rates of O_3 and NO_2. This allows calculations of OH using a zero dimensional time dependent model. The modelled OH concentrations significantly exceed the measured values for low NO_x concentrations. It is argued that additional, so far unidentified, HO_x loss reactions must be responsible for that discrepancy.

Key words. OH-radicals, troposphere, long path absorption spectroscopy, sensitivity study, formaldehyde, measurements.

1. Introduction

The reaction of the hydroxyl radical, OH, with atmospheric trace gases is one of the most important chemical processes in the troposphere. In many cases that reaction provides the first and rate limiting step in the chain of oxidation reactions which eventually break down a given trace gas molecule. Consequently, the concentration of OH determines the atmospheric life time, and thus the concentration of a large variety of atmospheric trace gases. In turn these trace gases influence the OH concentration, and the chemistry of OH is coupled

more or less strongly to nearly all trace gas cycles. As a consequence the chemistry of OH is complex; the prediction of its concentration by numerical models must necessarily be based on incomplete knowledge of the trace gases present and reactions involved, and is, therefore, subject to large uncertainties. Experimental field tests of the model predicted OH concentrations are badly needed.

There are a few published OH measurements made more or less locally by various techniques (Wang *et al.*, 1975; Davis *et al.*, 1976, 1979a, b, 1985; Perner *et al.*, 1976; Hübler *et al.*, 1984; Campbell *et al.*, 1979; Sheppard *et al.*, 1982; Watanabe *et al.*, 1982; Hard *et al.*, 1984; Rodgers *et al.*, 1985). Although the more reliable of these measurements gave OH concentrations of a few 10^6 cm^{-3}, which is in general agreement with various published model predictions, they hardly constitute a model test, because the actual chemical state of the atmosphere, in which these OH measurements were made, was not characterized by auxiliary measurements. In addition, there are estimates of the globally averaged OH concentration based on the budget of CH_3CCl_3 and ^{14}CO, which give numbers around 0.5×10^6 cm^{-3} (*cf.* Crutzen and Gidel, 1983, Derwent and Eggleton, 1981; Volz *et al.*, 1981). Although these can serve as a general constraint, they do not test our knowledge of the OH chemistry either, because such a global average extends over many different environments whose trace gas distributions are insufficiently established and whose contributions to the global OH-average are therefore uncertain. For instance, the global background concentrations of NO and NO_2 are not known, but essential for calculating OH.

In this paper we present new OH measurements by groundbased laser long path UV absorption spectroscopy, the technique we had used before (Hübler *et al.*, 1984). Moreover, we simultaneously measured most of the parameters and trace gas concentrations which are thought to determine the tropospheric OH concentration. Our field experiments observed air masses with light to moderate pollution providing an order of magnitude range in NO_x concentration and a somewhat lesser range for the other trace gases. Hence, for the first time, we can attempt to compare measured OH concentrations to those modelled for a chemically well characterized range of airmasses.

2. Basic OH Chemistry

To define those parameters which determine the tropospheric OH concentration, and the measurement of which is therefore essential, we give a brief outline of the basic OH chemistry. The reactions influencing the OH concentration can be broadly classified into four categories: The production reactions of OH, the reactions converting OH to the hydroperoxy radical, HO_2, the reactions cycling HO_2 back to OH, and the radical–radical reactions which terminate the recycling chains and remove OH or HO_2 from the atmosphere. In the following each of the categories will be illustrated by examples of the

most important reactions acting in the chemical environment encountered in our experiments (i.e. $NO_x \geqslant 1$ ppb).

The primary and most important production of OH virtually everywhere in the troposphere proceeds through the UV photolysis of ozone, which yields excited oxygen atoms, $O(^1D)$,:

$$O_3 + h\nu \rightarrow O(^1D) + O_2\,(^1\Delta_g) \qquad \lambda \leqslant 320 \text{ nm} \tag{1}$$

The resulting $O(^1D)$ are mostly quenched by N_2 and O_2 to form the ground-state oxygen atom, $O(^3P)$:

$$O(^1D) + N_2 \rightarrow O(^3P) + N_2 \tag{2}$$

$$O(^1D) + O_2 \rightarrow O(^3P) + O_2 \tag{3}$$

But a significant fraction of $O(^1D)$, between 1% and 10% in the planetary boundary layer, reacts with water vapor to form OH:

$$O(^1D) + H_2O \rightarrow OH + OH \tag{4}$$

The OH radicals react with a large variety of trace gases. The majority of those reactions eventually converts OH to HO_2. The most simple and the most important example of such a conversion reaction is that with carbon monoxide, CO,

$$OH + CO \rightarrow CO_2 + H \tag{5}$$

which is immediately followed by

$$H + O_2 + M \rightarrow HO_2 + M \tag{6}$$

to form the hydroperoxy radical, HO_2. This process had been proposed by Weinstock (1969), and was the first incentive for the search for tropospheric OH.

Another significant reaction, which eventually converts OH to HO_2, proceeds with methane as pointed out by Levy (1972).

$$OH + CH_4 \rightarrow H_2O + CH_3 \tag{7}$$

This reaction is immediately followed by

$$CH_3 + O_2 + M \rightarrow CH_3O_2 + M. \tag{8}$$

The resulting methylperoxyradical, CH_3O_2, reacts mainly with NO

$$CH_3O_2 + NO \rightarrow CH_3O + NO_2 \tag{9}$$

to form the methoxy radical CH_3O, which in turn reacts with O_2 to yield formaldehyde, CH_2O, and HO_2:

$$CH_3O + O_2 \rightarrow CH_2O + HO_2 \tag{10}$$

Analogous reactions occur in the oxidation of light non-methane hydrocarbons, NMHC, (Atkinson *et al.*, 1982) which in total can be more important than CH_4 (cf. Rudolph *et al.*, 1980; Ehhalt *et al.*, 1986).

By far the most important reaction cycling HO_2 back to OH is:

$$HO_2 + NO \rightarrow OH + NO_2, \tag{11}$$

and only for completeness and because it can be dominant in the background atmosphere we also mention the recycling reaction with O_3

$$HO_2 + O_3 \rightarrow OH + O_2 + O_2. \tag{12}$$

Reactions (5) to (10) and (11) interconvert OH and HO_2 so fast that both are virtually in photochemical equilibrium. For that reason they are often treated as a sum, HO_x.

The most important OH loss reaction in the airmasses encountered in our experiments is reaction with nitrogen dioxide, NO_2 to form nitric acid, HNO_3,

$$OH + NO_2 + M \rightarrow HNO_3 + M \tag{13}$$

other reactions contributing to the loss of HO_x are:

$$OH + HO_2 \rightarrow H_2O + O_2, \tag{14}$$

$$HO_2 + HO_2 \rightarrow H_2O_2 + O_2, \tag{15}$$

$$CH_3O_2 + HO_2 \rightarrow CH_3O_2H + O_2, \tag{16}$$

The peroxides, H_2O_2 and CH_3O_2H, are water soluble and partly removed from the atmosphere by heterogeneous processes. Furthermore the peroxides react with OH:

$$H_2O_2 + OH \rightarrow H_2O + HO_2 \tag{17}$$

$$CH_3O_2H + OH \rightarrow H_2O + CH_3O_2 \tag{18}$$

These reactions together with reaction (15) and (16), respectively, catalyze reaction (14). Nevertheless in the airmasses observed here, the HO_x loss from all the reactions (14) to (18) should be considerably smaller than that from reaction (13) alone.

There is one more point which needs to be addressed when making field experiments. The intermediate products of atmospheric oxidation processes, namely CH_2O, H_2O_2, CH_3O_2H or other alkylhydroperoxydes and carbonyls are also sources of HO_x, because they are photolysed at UV wavelengths penetrating to the earth's surface:

$$H_2O_2 + h\nu \rightarrow OH + OH \tag{19}$$

$$CH_3O_2H + h\nu \rightarrow CH_3O + OH \tag{20}$$

the latter followed by reaction (10) to convert CH_3O into $HO_2 + CH_2O$. Finally CH_2O can be photolyzed:

$$\rightarrow H_2 + CO \qquad (21a)$$

$$CH_2O + h\nu \rightarrow HCO + H \qquad (21b)$$

The formyl radical, HCO, formed in reaction (21b) reacts with O_2 to yield HO_2

$$HCO + O_2 \rightarrow HO_2 + CO \qquad (22)$$

and the H-atom reacts via reaction (6).

In photochemical steady state these secondary HO_x sources should be weaker than the primary source from O_3 photolysis. However, the air mass actually observed could have originated from a highly polluted area and carry with it large concentrations of CH_2O, and higher carbonyls, all of which have lifetimes of half a day or more and are therefore readily transported over large distances. These elevated concentrations could give rise to unaccounted OH production. Therefore, at least one of the carbonyls, the concentrations of which vary more or less in parallel, should be measured.

From this outline we can derive the following requirements for the auxiliary measurements: It is essential that the primary production of OH via reactions (1) and (4) be determined. This requires the measurement of the O_3 photolysis rate, J_1, and the measurement of the O_3 and H_2O concentrations.

It is also essential that the dominant losses of HO_x be determined. In the air masses investigated, which had relatively high NO_x concentration, this loss is mostly due to reaction (13), and this task is largely reduced to the measurement of the NO_2 concentration.

The other HO_x loss reactions involve HO_2. Thus it is next in importance to measure HO_2, or the parameters which control the partitioning between OH and HO_2. This requires the additional measurement of CO, CH_4, NMHC, and H_2 for the conversion of OH to HO_2 and that of NO (or the photolysis frequency of NO_2, J_{32}) for the inverse conversion. It would also be useful to measure RO_2 (*cf.* reaction (16)).

Finally it would be useful to measure at least one of the secondary source gases of OH, i.e. H_2O_2, CH_3O_2H, or preferably, CH_2O, because the latter is the most important secondary source of HO_x under the conditions of our measurements.

3. Experimental

Altogether, four field campaigns were carried out: Three during the summers of 1980, 1981, and 1983 at Deuselbach, a small village in the Hunsrück Mountains (50° N, 7° E), and one during September 1982 at Jülich (51° N, 6.5° E), a relatively polluted site owing to its proximity to the industrial regions of Belgium and the Rhein–Ruhr District.

3.1. OH *Measurements*

OH was measured using long path absorption spectroscopy, LPA. The light source consisted of a mode-locked Argon ion laser which pumped a frequency-doubled dye laser. It emitted a broad line at 308 nm wavelength encompassing the strong $Q_1(2)$ and the weaker $Q_{21}(2)$ line of the OH absorption spectrum. The OH absorption signal superimposed on the laser light after a 10 km passage through the free atmosphere was resolved by a double monochromator with a mechanical scanning system and recorded by an electronic data collection system. The method, calibration, data handling and accuracy have been described in detail by Hübler *et al.* (1984).

In 1980 and 1981 the OH instrument and the measurement site were exactly the same as those described by Hübler *et al.* (1984). Figure 1 shows the terrain at Deuselbach and the position of the light path. The latter had an average height of about 80 m above ground, which was mostly covered by deciduous and coniferous trees except for a stretch, about 25%, of agricultural land. The laser light source was housed in a truck parked near an air monitoring station of the Umweltbundesamt, UBA. This station also housed the *in situ* measuring apparatus. The laser light was reflected by a plane mirror mounted on the plat-

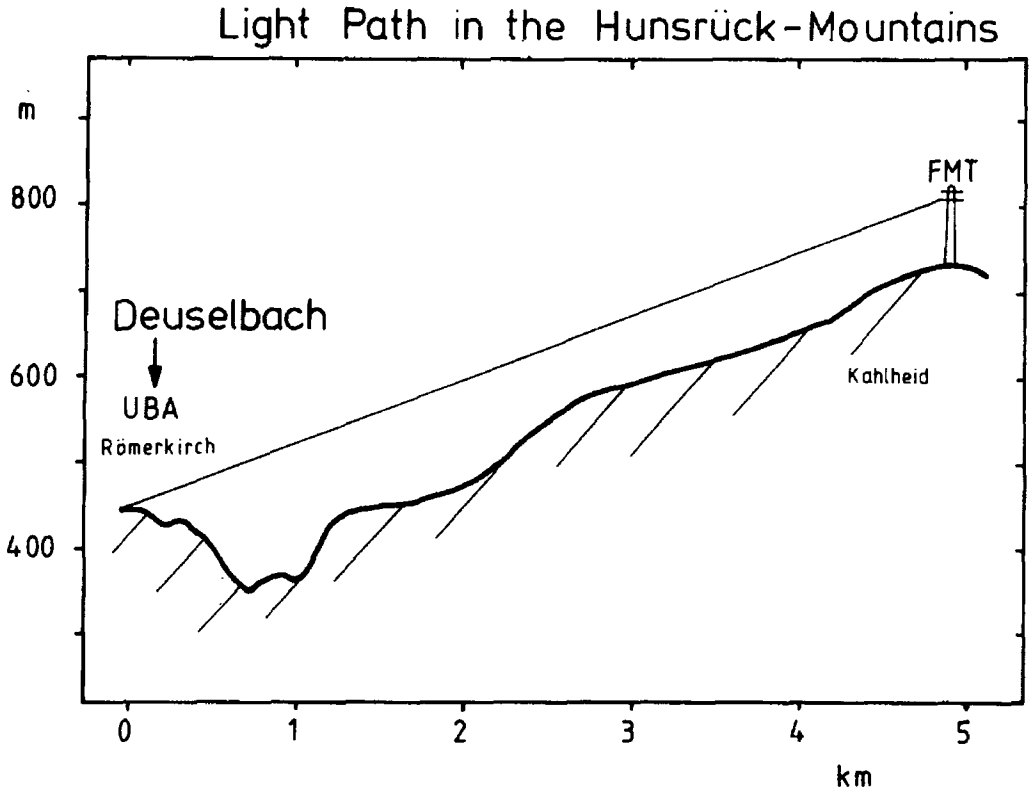

Fig. 1. Light path and terrain at Deuselbach. The laser was positioned at the UBA station, 480 m above sea level, 7° 3′ 15″ E longitude, 49° 45′ 45″ N latitude. The mirror was located at the tower, 810 m above sea level, 7° 7′ 10″E, 49° 45′ 3″ N.

form of a telecommunication tower (FMT) at 4.8 km distance, giving a total path length of 9.6 km.

During September 1982 in Jülich a somewhat improved version of the OH experiment was used. The temperature tuned frequency doubling crystal (ADA) was replaced by an angle tuned $LiIO_3$ crystal, resulting in a 10-fold improved UV output of the laser system of about 10 mW. In addition, a new 12-bit analog/digital converter (MOD 1205 from Analog Devices) provided a much larger dynamic range of the receiving system than the earlier 8-bit device. The light path of that OH experiment extended north of the town from a laboratory at the Fachhochschule Aachen Abteilung Jülich. It ran at an average height of about 10 m above ground, all of which was agricultural land, and was reflected by a mirror sited at a distance of 5.2 km. At that point a container housed the *in situ* instrumentation and the Xenon-arc light source for the auxiliary LPA experiment.

In 1983, at Deuselbach the instruments were positioned as in 1981 (see Figure 1) and the improved OH experiment was used.

3.2. *Supplementary Trace Gases*

Of the compounds identified as important, we measured O_3, H_2O, NO, NO_2, CO, CH_4, CH_2O and the light nonmethane hydrocarbons (NMHC). The techniques used and their uncertainties have also been documented in earlier papers. They are listed together with their estimated uncertainties and references in Table I. In the following we add a few remarks on the geographical position of the auxiliary measurements.

During all OH-measurements the beam from a Xenon-arc light source of a second LPA instrument was running parallel the full length of the laser beam of the OH instrument at a distance of 10 m to 50 m. The light of the auxiliary LPA experiment passed the distance only once – in the case of Deuselbach from the Xenon-arc lamp mounted on the tower to the spectrometer located at the UBA station. This second LPA instrument served to measure NO_2, O_3, CH_2O and SO_2 in virtually the same air mass in which OH was measured. These gases were also measured by *in situ* techniques (*cf.* Table I) at one end of the light beam – in Deuselbach at the UBA monitoring station. That redundancy in techniques provided a useful check on the homogeneity of the trace gas distributions along the light path. The mixing ratios of carbon monoxide and the hydrocarbons were determined by gas chromatographic analysis of grab samples collected during the OH measurements at the site of the *in situ* measurements. Beginning in 1983 the CO mixing ratio was also monitored at hourly intervals by an automated gas chromatograph at the site. Until 1981 the highest NMHC measured were C_5. Thereafter the range of NMHC was extended to C_{10}, with particular attention to the light aromatic hydrocarbons.

In addition meteorological data, namely pressure, temperature, relative

Table I. Measured parameters and the techniques used for measurement. LPA stands for long path absorption spectroscopy.

Parameter	Technique	Error (%)	References
OH	Laser LPA	see Table II	Hübler *et al.*, 1984
O_3	LPA, ultraviolet	10	Platt and Perner, 1983
	Optical absorption (Dasibi)		
	Chemiluminescence		
NO, NO_2	Chemiluminescence	20	Ridley and Howlett, 1974
			Helas *et al.*, 1981
			Drummond *et al.*, 1985
NO_2	LPA, ultraviolet	10	Platt and Perner, 1983
CH_2O	LPA, ultraviolet	10	Platt and Perner, 1983
	Derivation/HPLC		Lowe *et al.*, 1983
SO_2	LPA, ultraviolet	10	Platt and Perner, 1983
	Iodometry	10	Rumpel, 1982
H_2O	Psychrometer	5	
	LPA, visible		Platt and Perner, 1983
Hydrocarbons	Gaschromatography	10	Rudolph *et al.*, 1981
CO	Gaschromatography	5	Rudolph *et al.*, 1981
J_1	Photoelectric Detector	20	Junkermann *et al.*, 1986
J_{32}	Photoelectric Detector	20	Junkermann *et al.*, 1986

humidity, wind speed, wind direction, and total radiation, were continuously recorded by a computer controlled system at the site of the in situ measurements.

3.3. *Photolysis Frequencies*

Beginning 1982 the photolysis frequencies of O_3 to yield $O(^1D)$, J_1, and of NO_2 to yield NO and $O(^3P)$, J_{32}, were continuously recorded by photoelectric detectors at the site of the *in situ* measurements. The spectral response of the detectors was adjusted to match the wavelength dependence of the product of the absorption crossection and quantum yield (both taken from NASA, 1985) of each one of the two gases. Unfortunately, in both campaigns the photoelectric detectors had not yet been calibrated. Thus the absolute spectral photon flux for clear skies had still to be calculated. This was done for sea level and 50° N latitude using the standard solar photon flux (NASA, 1979), a ground albedo of 0.1 and the actual ozone column densities measured at Hohenpeißenberg (Deutscher Wetterdienst, 1981–1983). The effects of Rayleigh- and Mie-scattering were also included according to Anderson and Meier (1979). At the standard case, which corresponded to a surface visibility of 25 km at 550 nm wavelength, the influence of Mie-scattering was about 10%. The thus calculated photon flux at the earth's surface and 50° N latitude was used to normalize the signal of the photoelectric detectors for clear sky conditions. Used in this mode,

the photoelectric detector essentially monitored the influence of cloud cover and strong haze on the photolysis frequencies (*cf.* Figures 4 and 5). The resulting photolysis frequencies are included in Table III.

4. Experimental Results

The OH concentration is determined from the absorption of its $Q_1(2)$ line at 307.995 nm. That absorption feature becomes discernible after the curvature of the laser line profile and the usually stronger absorption features by SO_2 are removed from the original spectra – the former by division through a seventh order polynomial fit to the observed spectrum, the latter by subtracting a properly scaled SO_2 reference spectrum (Hübler *et al.*, 1984). (This procedure also

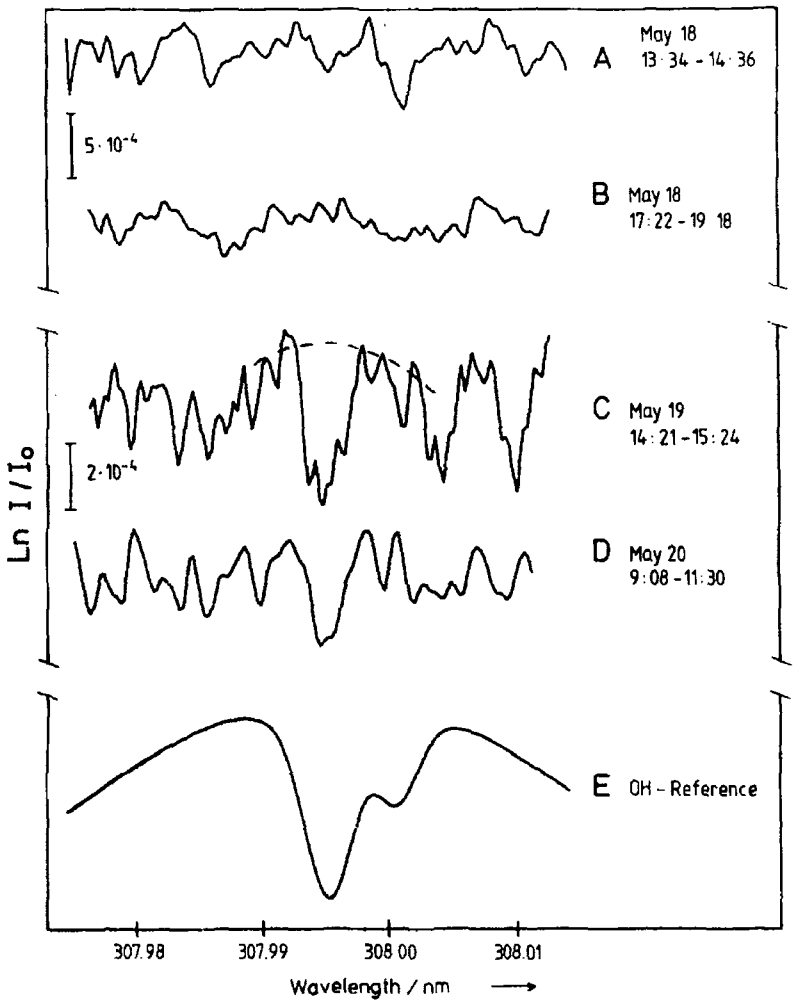

Fig. 2. Traces A–D: Reduced OH absorption spectra obtained at Deuselbach during May 1983. The total light path was 9.6 km. Spectra C and D carry an OH signal; spectrum B does not. Spectrum C shows additional unidentified features at 308.003 nm and 308.010 nm. The dashed line in C indicates the baseline under the Q_1 (2) line of OH. E represents an OH flame spectrum for reference. Time is given in central European time (CET).

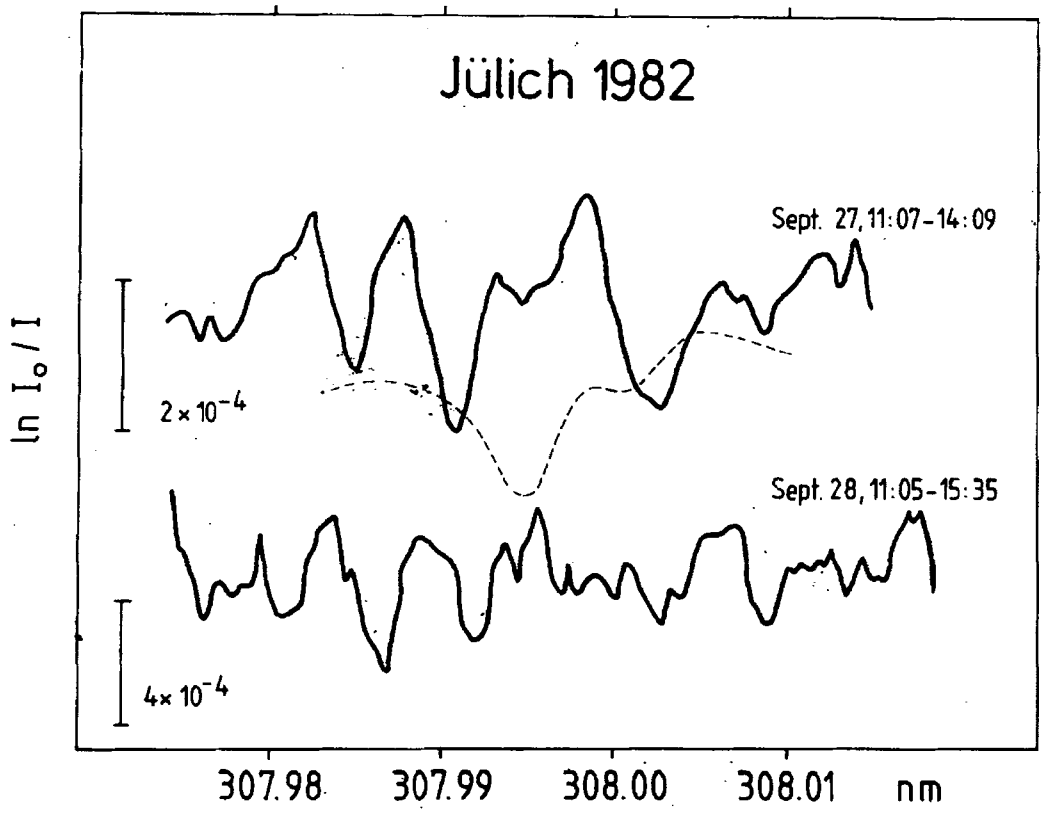

Fig. 3. Reduced OH absorption spectra obtained at Jülich during September 1982. The total light path was 10.4 km. Both spectra mainly exhibit unidentified absorption features. Time is given in CET.

allows determination of the SO_2 concentration. At sufficiently high SO_2 levels that SO_2 measurement agrees within 5% with that measured directly by the second LPA instrument.) Examples of the resulting residual spectra from the current measurements are shown in Figures 2 and 3. Not all of these spectra show a significant signal from OH. Examples are the spectra A and B in Figure 2, which were obtained in Deuselbach on May 18, 1983 at 13:34–14:36 and 17:22–19:18, respectively. In the latter case, actually no OH signal would be expected, because the OH-production in the evening is small. This spectrum is included as a blank to indicate the noise of the base line. Spectra C and D, from May 19, 14:21–15:24, and May 20, 9:08–11:30, carry OH signals. The depths of the differential absorption are 4.6×10^{-4} and 3×10^{-4} corresponding to OH concentrations of 3.2×10^{6} and 1.9×10^{6} cm^{-3}.

It is noted that the baseline will be curved in a convex manner, if the residual spectrum is dominated by a single absorption feature, as is emphasized by the dashed line in trace C of Figure 2. This is an artifact of the fitting routine, which in its attempt to minimize the total deviation of the fitted polynomial from the observed spectrum tends to overcompensate at the sections adjacent to that feature.

We also note that spectrum C shows additional lines at 308.003 nm and 308.010 nm, which we suspect to be absorption features of a hitherto unknown species. Further and even stronger lines were observed in some of the spectra obtained over Jülich, 1982, as demonstrated in Figure 3. About every third of the OH spectra obtained in the present field campaigns appeared to have additional absorption features. They occurred at different wavelengths and varied in relative strength, which would point to a varying mix of different species. Absorption lines in the spectral range around the $Q_1(2)$ line besides those from SO_2 are known to exist, for example due to CS_2 and CH_2O (Hübler *et al.*, 1984). Those features, however, occur at wavelengths of 307.985 nm, 308.001 nm, 308.018 nm, and 307.982 nm, 307.992 nm, 308.005 nm, respectively, and fail to explain the current observations. Thus, the absorption features can not be assigned and we have – at least in principle – to admit the possibility that they could be due to random fluctuations in the baseline. In any case they have to be included in the uncertainty of the OH measurement to account for the possibility that such a fluctuation might also appear at the wavelength of the $Q_1(2)$ line and cause a spurious OH signal. In order to be conservative, therefore, the root mean square noise of the baseline, which is mainly responsible for the uncertainty of the OH signal, was calculated treating these lines as additional noise. In this way the 1σ errors in the OH concentration from spectrum C and D in Figure 2 are $\pm 1.1 \times 10^6$ cm^{-3} and $\pm 0.9 \times 10^6$ cm^{-3}, respectively. The 1σ errors in spectrum A and B amount to $\pm 2.3 \times 10^6$ cm^{-3} and $\pm 1.2 \times 10^6$ cm^{-3}.

The OH concentrations measured during the field campaigns from 1980 to 1983 and their errors are summarized in Table II. In the cases, where the 1σ error significantly exceeds the signal, only an upper limit is given consisting of the sum of signal and the 1σ error. The data can be categorized with respect to the synoptic situation and pollution levels as follows. Deuselbach is a relatively remote rural station, and low levels of pollution with NO_2 mixing ratios less than 1 ppb are frequently encountered. However, during the two campaigns in September 1980 and July/August 1981 a stable high pressure system controlled the circulation over Central Europe and the air masses arriving at Deuselbach had passed over industrial areas. Thus relatively high pollution levels prevailed with NO_2 and SO_2 mixing ratios reaching several ppb (see Table III, No. 1–5). On August 6, even the aerosol content reached atypically high levels. During those campaigns the OH radical concentration remained always below the experimental detection limit, which varied between 0.7×10^6 and 2×10^6 cm^{-3} (Table II).

Elevated pollution levels were also encountered during the measurements at Jülich (see Table III, No. 6–10), and only upper limits for the OH concentration could be deduced.

During the campaign at Deuselbach in 1983 subsiding air masses provided good visibility and low pollution levels. For example at May 19 and 20 the

Table II. OH concentration measurements.

No.	Date	Time CET	[OH] measured (10^6 cm^{-3})
	1980 Deuselbach		
1	Sept. 24	11:00–12:30	<2.0*
	1981 Deuselbach		
2	July 29	13:50–16:00	<1.5*
3	Aug. 6	14:25–16:50	≤1.1*
4	Aug. 25	12:50–15:40	≤1.3*
5	Aug. 27	13:50–16:40	<0.6*
	1982 Jülich		
6	Sept. 27	11:07–14:09	<1.6
7	Sept. 27	14:10–15:40	<0.7
8	Sept. 28	11:05–13:53	<0.7
9	Sept. 28	13:53–15:35	<1.7
10	Sept. 29	11:12–12:50	<1.3
	1983 Deuselbach		
11	May 16	15:50–18:19	<1.7
12	May 17	09:53–11:24	2.2 ± 2.3
13	May 18	11:37–13:28	1.2 ± 1.7
14	May 18	13:34–14:36	2.1 ± 2.3
15	May 18	14:41–17:17	1.5 ± 1.2
16	May 18	17:22–19:18	<1.2
17	May 19	12:07–14:19	2.9 ± 1.3
18	May 19	14:21–15:24	3.2 ± 1.1
19	May 19	15:27–16:29	1.0 ± 0.6
20	May 20	09:08–11:30	1.9 ± 0.9
21	May 20	11:31–13:05	0.7 ± 1.2
22	May 20	13:06–14:30	≤1.4
23	May 20	14:31–15:48	≤1.5

* from Hübler *et al.*, 1984 but using 1σ-upper limits.

NO_2 and SO_2 mixing ratios were of the order of one ppb (see Table III). Under those conditions we observed our highest OH concentrations so far (up to 3.2×10^6 cm^{-3}).

During that campaign also up to four OH measurements per day were obtained. They are plotted in Figures 4 and 5 together with the measurements of O_3, NO_2, CH_2O and the ozone photolysis frequency, J_1, to give an impression of the diurnal variation. During the afternoon of May 19 (Figure 4) the NO_2 concentration decreased from 1 ppb to 0.6 ppb and so did J_1 from about 1.5×10^{-5} sec^{-1} to 0.6×10^{-5} sec^{-1}. The measured OH concentration dropped from about 3×10^6 cm^{-3} between 12:30–15:30 hours to 1×10^6 cm^{-3} around 16:00. The next day (May 20, Figure 5) higher NO_2 levels (0.7 to 3.1 ppb) prevailed, and J_1 ranged up to 2×10^{-5} sec^{-1}. The measured OH concentration, however, did not exceed 1.9×10^6 cm^{-3} during the whole day.

On all the dates when OH measurements were made, a more or less complete set of auxiliary measurements was also obtained. Tables III and IV give

Table III. Auxiliary measurements of trace gas concentrations and parameters required for the model calculation of the OH concentration. The last columns for NO_2 and NO represent the values entered in the model calculations.

No.	Date	Dobson	J_1 (10^{-5} sec^{-1})	J_{32} (10^{-3} sec^{-1})	O_3[a] ppb	CO ppb	H_2O (10^{17} cm^{-3})	Temp. °C	SO_2[a] ppb	Aeros. μgm^{-3}	CH_2O[a] ppb	CH_2O[c] ppb	NO_2[a] ppb	NO_2[b] ppb	NO[b] ppb	NO_2 ppb	NO ppb
	1980 Deuselbach																
1	Sept. 24	283	0.85	5.9	43	220	2.6	–	9	–	–	–	–	3.8	2.2	4.6	1.4
	1981 Deuselbach																
2	July 29	315	1.26	7.1	45	140	3.4	22.4	2.9	32	<4	–	–	2.3	1.1	2.5	0.9
3	Aug. 6	296	0.95	6.3	85	310	3.5	27.5	6.7	80	<3	–	2.0	–	0.28	2.0	0.3
4	Aug. 25	311	1.11	6.8	43	250	2.2	17.5	6.7	49	<1.6	–	2.0	4.1	1.9	2.0	0.8
5	Aug. 27	310	0.73	5.9	28	210	2.9	16.5	8.6	49	<1.4	–	5.3	4.7	2.6	5.4	2.8
	1982 Jülich																
6	Sept. 27	283	0.82	5.8	30	180	3.28	19.3	19	–	–	0.7	10	–	4.5	9.9	4.6
7	Sept. 27	283	0.42	4.7	(30)	180	3.28	21.8	1.4	–	–	0.9	2.7	–	(1.4)	2.8	1.0
8	Sept. 28	282	0.82	5.8	36	160	3.12	20.0	1.4	–	–	0.8	3.2	–	1.2	3.2	1.2
9	Sept. 28	282	0.41	4.7	48	140	2.99	22.0	1.4	–	–	0.9	4.1	–	1.2	4.3	1.5
10	Sept. 29	270	0.88	5.8	30	190	3.74	21.0	2.4	–	–	1.8	5.1	–	2.2	5.1	1.5
	1983 Deuselbach																
11	May 16	303	0.32	4.4	42	320	3.0	17.0	9.3	–	0.4	–	6.7	–	–	6.9	1.8
12	May 17	326	0.78	3.6	41	320	2.74	14.5	5.3	–	0.9	–	2.2	–	–	2.3	0.6
13	May 18	336	1.64	7.6	40	270	2.11	17.2	–	–	–	–	–	7.8	2.3	6.9	3.2
14	May 18	336	1.08	5.7	42	280	2.08	17.0	9.0	–	–	–	–	3.6	1.1	3.5	1.2
15	May 18	336	0.55	5.0	46	240	1.96	17.2	–	–	–	0.7	–	1.3	0.3	1.3	0.3
16	May 18	336	0.06	2.6	46	230	1.81	15.1	–	–	–	0.7	–	2.4	0.16	2.2	0.3
17	May 19	341	1.26	6.2	48	230	2.10	15.0	0.7	–	0.3	0.4	1.0	1.0	0.3	1.0	0.3
18	May 19	341	0.97	6.1	50	210	2.03	16.2	0.7	–	0.3	0.4	0.6	0.9	0.26	0.6	0.2
19	May 19	341	0.67	5.9	52	210	1.96	16.4	0.5	–	0.3	0.5	0.6	0.75	0.18	0.6	0.2
20	May 20	321	1.14	6.5	53	260	2.27	18.5	1.6	–	0.5	0.9	1.6	1.0	0.33	1.6	0.5
21	May 20	321	1.86	8.0	57	250	2.13	21.9	1.5	–	0.6	–	1.5	1.0	0.31	1.5	0.5
22	May 20	321	1.31	6.1	58	290	2.08	21.5	1.3	–	0.5	–	0.7	0.55	0.17	0.7	0.2
23	May 20	321	0.36	2.2	62	250	2.06	18.0	1.8	–	0.4	–	3.1	1.1	0.3	3.2	0.3

[a] = measured by long path absorption spectroscopy (value averaged over ~5 km light path)
[b] = measured by chemiluminescence (*in situ* measurement)
[c] = measured by derivatisation/HPLC (*in situ* measurement).

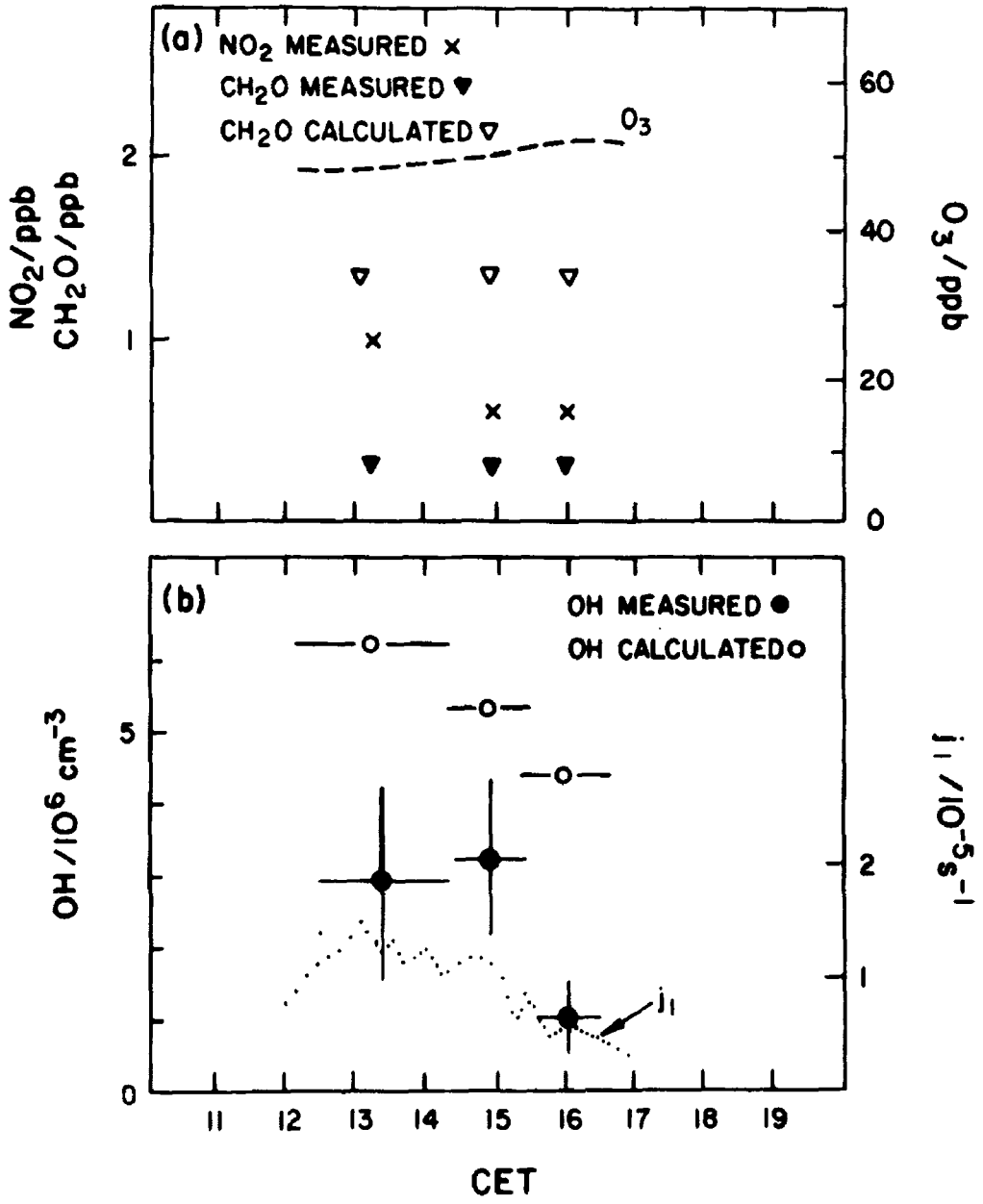

Fig. 4. Diurnal variation of the measured OH concentration, NO_2, O_3, and CH_2O mixing ratios on May 19, 1983 at Deuselbach. For comparison the model calculated values of OH and CH_2O are also shown. The dotted line (lower panel) represents the O_3 photolysis frequency, J_1.

the values averaged over the time intervals of the individual OH measurements. This averaging presented no problem for the parameters measured continuously (J_1, J_{32}, O_3 (DASIBI), H_2O and NO, NO_2 by chemiluminescence). Also the LPA-measurements of NO_2, SO_2, O_3, and CH_2O were made at 20 min integration time intervals and thus will give a good approximation to the average concentrations, of those species during the time interval of the OH measurements. For the hydrocarbon data the situation is less satisfactory, since only between one and three grab samples were taken per day. Moreover, being

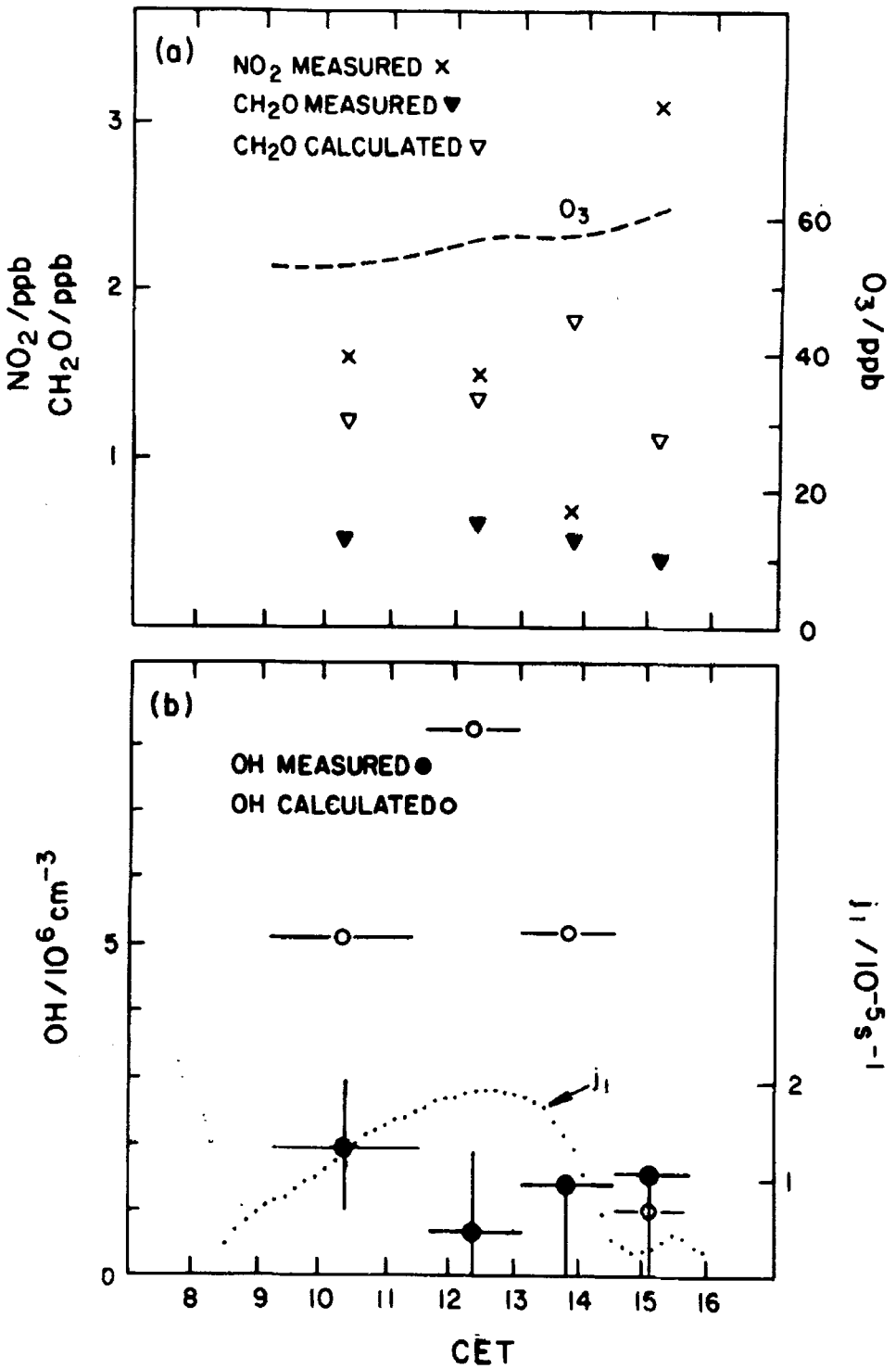

Fig. 5. Diurnal variation of the measured OH concentration, NO_2, O_3, and CH_2O mixing ratios on May 20 at Deuselbach. For comparison the model calculated values of OH and CH_2O are also shown. The dotted line (lower panel) represents the O_3 photolysis frequency, J_1.

instantaneous measurements, they might not necessarily reflect the average hydrocarbon concentrations during the time interval of the OH measurements.

Table IV. Measured mixing ratios of C_1–C_5 Hydrocarbons (in ppb).

No.	Date	CH_4	C_2H_2	C_2H_4	C_2H_6	C_3H_6	C_3H_8	*i*But.	*n*But.	*i*Pent.	*n*Pent.
	1980 Deuselbach										
1	Sept. 24	–	–	–	–	–	–	–	–	–	–
	1981 Deuselbach										
2	July 29	1650	0.3	1.5	1.9	0.75	0.2	0.06	0.08	–	–
3	Aug. 6	1680	1.1	0.6	3.7	0.07	1.0	0.3	0.5	0.5	0.2
4	Aug. 25	1700	0.6	1.1	1.5	0.075	0.8	0.14	0.2	0.2	0.07
5	Aug. 27	1640	0.3	0.9	1.3	0.23	0.4	0.07	0.11	0.1	0.04
	1982 Jülich										
6	Sept. 27	1640	–	–	–	–	–	–	–	–	–
7	Sept. 27	1640	–	–	2.9	4.4	1.0	0.6	0.45	1.27	0.66
8	Sept. 28	1640	0.2	–	2.04	0.1	0.54	0.25	0.63	0.46	0.24
9	Sept. 28	1660	0.3	0.26	2.04	0.1	0.47	0.17	0.43	0.33	0.13
10	Sept. 29	1640	0.8	0.33	2.77	0.2	0.57	0.28	0.63	0.43	–
	1983 Deuselbach										
11	May 16	–	–	–	–	–	–	–	–	–	–
12	May 17	–	–	–	–	–	–	–	–	–	–
13	May 18	–	–	–	–	–	–	–	–	–	–
14	May 18	–	–	–	–	–	–	–	–	–	–
15	May 18	1710	0.56	0.61	3.1	0.13	0.45	0.13	0.27	0.17	0.08
16	May 18	–	–	–	–	–	–	–	–	–	–
17	May 19	–	–	–	–	–	–	–	–	–	–
18	May 19	–	–	–	–	–	–	–	–	–	–
19	May 19	1710	0.39	0.35	2.1	0.06	0.38	0.08	0.22	0.13	0.08
20	May 20	–	–	–	–	–	–	–	–	–	–
21	May 20	1740	0.68	0.33	2.1	0.05	0.54	0.22	0.48	0.40	0.15
22	May 20	1750	0.86	0.66	2.3	0.09	0.67	0.31	0.67	0.50	0.22
23	May 20	1760	0.63	0.32	2.5	0.07	0.58	0.23	0.46	0.33	0.13

5. The Model and Its Results

A time dependent zero dimensional model was used for the calculation of the OH concentrations. The photochemistry of the model is based on the usual complement of reactions (NASA, 1985), e.g. reactions (1) to (22) given above, supplemented by reactions (23) to (39) given in Table V. The chemistry of the alkanes up to butane and of the olefins C_2H_4 and C_3H_6 was included utilizing the schemes proposed by Atkinson *et al.* (1982). A complete list of the reactions, their rates and products can be found in Liu *et al.* (1986). It is noted that we used net reactions, wherever feasible without loss of information or accuracy, and that the individual NMHC reactions are not listed but only represented by the token reactions (30) and (31) in Table V. To consider surface deposition of HNO_3, a constant loss term was assumed (Table V).

The measured parameters served as input to the model. Thus the mixing ratios of O_3, H_2O, CO, CH_4, NMHC, NO_2 (listed in Table III) were prescribed, but not CH_2O and NO. The latter, although measured by *in situ* chemiluminescence, was calculated from the NO_2 measured by LPA. This was done

Table V. Reactions and rate constants (298 K, $p = 1$ atm) used for the calculation of OH concentration.

Reaction			Rate constant (molec cm^{-3} sec^{-1})	Error factor
1	$O_3 + h\nu$	$\rightarrow O(^1D) + O_2\ (^1\Delta_g)$	J_1	
2	$O(^1D) + N_2$	$\rightarrow O(^3P) + N_2$	2.6×10^{-11}	1.2
3	$O(^1D) + O_2$	$\rightarrow O(^3P) + O_2$	4.0×10^{-11}	1.2
4	$O(^1D) + H_2O$	$\rightarrow OH + OH$	2.2×10^{-10}	1.2
5	$OH + CO$	$\rightarrow H + CO_2$	2.4×10^{-13}	1.25
6	$H + O_2 + M$	$\rightarrow HO_2 + M$	1.2×10^{-12}	1.2
7	$OH + CH_4$	$\rightarrow H_2O + CH_3$	7.7×10^{-15}	1.2
8	$CH_3 + O_2 + M$	$\rightarrow CH_3O_2 + M$	1.1×10^{-12}	1.2
9	$CH_3O_2 + NO$	$\rightarrow CH_3O + NO_2$	7.6×10^{-12}	1.2
10	$CH_3O + O_2$	$\rightarrow CH_2O + HO_2$	1.5×10^{-15}	2.0
11	$NO + HO_2$	$\rightarrow NO_2 + OH$	8.3×10^{-12}	1.2
12	$O_3 + HO_2$	$\rightarrow O_2 + O_2 + OH$	2.0×10^{-15}	1.5
13	$OH + NO_2 + M$	$\rightarrow HNO_3 + M$	1.15×10^{-11}	1.26
14	$OH + HO_2$	$\rightarrow H_2O + O_2$	1.1×10^{-10}	1.5
15	$HO_2 + HO_2 + H_2O$	$\rightarrow H_2O_2 + O_2 + H_2O$	4.6×10^{-12} [a]	1.3
16	$CH_3O_2 + HO_2$	$\rightarrow CH_3O_2H + O_2$	6.0×10^{-12}	3.0
17	$OH + H_2O_2$	$\rightarrow H_2O + HO_2$	1.7×10^{-12}	1.3
18	$CH_3O_2H + OH$	$\rightarrow H_2O + CH_3O_2$	1.0×10^{-11}	2.0
19	$H_2O_2 + h\nu$	$\rightarrow OH + OH$	J_{19}	
20	$CH_3O_2H + h\nu + O_2$	$\rightarrow CH_2O + OH + HO_2$	J_{20}	
21a	$CH_2O + h\nu$	$\rightarrow H_2 + CO$	J_{21a}	
21b	$CH_2O + h\nu$	$\rightarrow H + HCO$	J_{21b}	
22	$HCO + O_2$	$\rightarrow HO_2 + CO$	5.5×10^{-12}	1.3
23	$OH + H_2$	$\rightarrow H_2O + H$	6.7×10^{-15}	1.2
24	$OH + O_3$	$\rightarrow HO_2 + O_2$	6.8×10^{-14}	1.3
25	$CH_2O + OH$	$\rightarrow H_2O + HCO$	1.0×10^{-11}	1.25
26	$O_3 + NO$	$\rightarrow NO_2 + O_2$	1.8×10^{-14}	1.2
27	$CH_3O_2 + CH_3O_2 + O_2$	$\rightarrow 2\,CH_2O + 2\,HO_2$	3.4×10^{-13} [b]	1.25
28	$HNO_2 + h\nu$	$\rightarrow OH + NO$	J_{29}	
29	$OH + NO + M$	$\rightarrow HNO_2 + M$	4.9×10^{-12}	1.8
30	$OH + NMHC + O_2$	$\rightarrow RO_2 + H_2O$	[d]	
31	$RO_2 + NO + O_2$	$\rightarrow NO_2 + HO_2 +$ Aldehyde/Ketone	[d]	
32	$NO_2 + h\nu$	$\rightarrow NO + O(^3P)$	J_{32}	
33	$O(^3P) + O_2 + M$	$\rightarrow O_3 + M$		
34	$OH + CH_3CHO + O_2$	$\rightarrow CH_3COO_2 + H_2O$	1.6×10^{-11}	
35	$CH_3COO_2 + NO_2$	$\rightarrow$ Peroxyacetylnitrate (PAN)		
35a	$PAN + M$	$\rightarrow NO_2 + CH_3COO_2 + M$	3.7×10^{-4}	
36	$OH + X$	$\rightarrow$ products	0.5[c]	–
37	$HO_2 + X$	$\rightarrow$ products	0.02[c]	–
38	$CH_3O_2(RO_2) + X$	$\rightarrow$ products	0.02[c]	–
39	HNO_3	$\rightarrow$ heterogenous loss	1.0×10^{-5}	–

[a] k_{15} includes water vapor (1% by volume) dependence (Kircher and Sander, 1984), this leads to smaller (about 10%) OH concentration for low NO_x levels, whereas the influence at higher NO_x is negligible.

[b] Reaction (27) showed to have no noticeable influence upon OH so that the reactions

$$CH_3O_2 + CH_3O_2 \rightarrow CH_2O + CH_3OH + O_2$$

$$CH_3O_2 + CH_3O_2 \rightarrow CH_3OOH + O_2 + \cdots$$

were omitted from the model.

[c] Hypothetical reactions removing OH, HO_2 and CH_3O_2.

[d] See Atkinson *et al.*, 1982.

because the NO concentration measured *in situ* was considered less representative for the air mass along the path of the OH experiment, as was indicated by occasional but significant differences in the NO_2 concentration observed by the two techniques. In the few cases where NO_2 measurements by LPA were not available (measurements 1, 2, 13–16), the NO_x concentration measured *in situ* was used as model input. The actual NO and NO_2 input concentrations for the calculations are also listed in Table III. The mixing ratio of molecular hydrogen, H_2, which was not monitored, was assumed constant at a level of 500 ppb.

The empirically determined photolysis frequencies for O_3 and NO_2, J_1 and J_{32} were also prescribed (see Table III). The other photolysis frequencies were obtained by appropriate scaling.

Besides OH, CH_2O and NO, the model also calculated the concentrations of those species which could not be measured. They include the peroxy-radicals HO_2, CH_3O_2 and RO_2 (where R stands for the C_2- to C_4-NMHC radicals), the aldehydes and ketones, and the peroxides H_2O_2 and CH_3O_2H. The times required to reach steady state differ markedly. While OH and NO reach steady state concentrations within minutes, CH_2O needs a few hours, H_2O_2 and CH_3O_2H several days. Therefore, the model was run for five full diurnal cycles with the measured input concentrations. Because NMHC measurements were not available for all OH measurements the model was run in two modes: One with CH_4 as the sole hydrocarbon, the other with all C_2 to C_4 hydrocarbons included. The results of the calculations are presented in Table VI. Besides OH, the calculated values for CH_2O, H_2O_2 and PAN are also shown. It is noted that the OH concentration from CH_4 as the sole hydrocarbon is always lower than that for the more complete set of NMHC, as is to be expected for the NO_x levels observed. However, with the exception of experiments No. 2, 4, and 15, the difference between the model runs is less than 20%. Thus the runs with CH_4 alone provide a rather close lower limit for the OH concentration calculated with the C_2–C_4 NMHC included. In contrast, the calculated CH_2O concentrations differ markedly – by at least a factor of two – between the two modes.

The model also lends itself to an analysis of the sensitivity of the OH concentration to a change in the varius input parameters. Such an analysis was carried out, to serve following purposes:

(a) to determine those parameters which influence the OH concentration most strongly;
(b) to estimate the uncertainty of the model predicted OH;
(c) to decide, which of the currently used measurement techniques has to be upgraded most urgently to reduce that uncertainty.

The analyses with respect to (a) confirm the qualitative conclusions reached in the section on the basic OH chemistry. In the following we deal mainly with

Table VI. Model results for the concentration of OH, CH_2O, H_2O_2, and PAN. For comparison the measured OH concentration is also included.

No.	Date	Time CET	[OH] (10^6 mol cm^{-3})		CH_2O ppb		H_2O_2 ppb	PAN ppb
		measured	[a]	[b]	[a]	[b]	[b]	[b]
	1980 Deuselbach							
1	Sept. 24	11:00–12:30	<2.0	1.1 ± 0.4	–	0.2	–	–	–
	1981 Deuselbach							
2	July 29	13:50–16:00	<1.5	4.1 ± 1.5	7.6 ± 2.1	0.54	4.62	–	–
3	Aug. 6	14:25–16:50	≤1.1	6.2 ± 1.8	6.8 ± 1.7	0.85	2.16	–	–
4	Aug. 25	12:50–15:40	≤1.3	2.9 ± 1.0	4.5 ± 1.6	0.46	1.77	–	–
5	Aug. 27	13:50–16:40	<0.6	0.6 ± 0.2	1.0 ± 0.4	0.25	1.0	–	–
	1982 Jülich							
6	Sept. 27	11:07–14:09	<1.6	0.5 ± 0.2	–	0.39	–	–	–
7	Sept. 27	14:10–15:40	<0.7	1.0 ± 0.4	–	0.42	–	–	–
8	Sept. 28	11:05–13:53	<0.7	1.6 ± 0.6	2.0 ± 0.9	0.45	1.0	0.09	0.24
9	Sept. 28	13:53–15:35	<1.7	0.6 ± 0.3	0.8 ± 0.3	0.36	0.8	0.09	0.05
10	Sept. 29	11:12–12:50	<1.3	1.4 ± 0.5	1.7 ± 0.6	0.4	0.8	0.09	0.1
	1983 Deuselbach							
11	May 16	15:50–18:19	<1.7	0.3 ± 0.1	–	0.27	–	–	–
12	May 17	09:53–11:24	2.2 ± 2.3	2.0 ± 0.7	–	0.4	–	–	–
13	May 18	11:37–13:28	1.2 ± 1.7	1.0 ± 0.3	–	0.13	–	–	–
14	May 18	13:34–14:36	2.1 ± 2.3	1.5 ± 0.6	–	0.3	–	–	–
15	May 18	14:41–17:17	1.5 ± 1.2	2.4 ± 0.7	3.6 ± 0.9	0.5	1.8	0.46	0.6
16	May 18	17:22–19:18	<1.2	0.2 ± 0.04	–	0.4	–	–	–
17	May 19	12:07–14:19	2.9 ± 1.3	5.7 ± 1.6	6.2 ± 1.6	0.5	1.2	0.46	0.46
18	May 19	14:21–15:24	3.2 ± 1.1	5.1 ± 1.3	5.3 ± 1.4	0.57	1.2	1.10	0.51
19	May 19	15:27–16:29	1.0 ± 0.6	4.0 ± 1.0	4.4 ± 1.2	0.57	1.2	1.12	0.53
20	May 20	09:08–11:30	1.9 ± 0.9	4.3 ± 1.2	5.1 ± 1.3	0.5	1.23	0.27	0.39
21	May 20	11:31–13:05	0.7 ± 1.2	7.4 ± 1.9	8.3 ± 2.1	0.6	1.32	0.33	0.48
22	May 20	13:06–14:30	≤1.4	5.4 ± 1.7	5.2 ± 1.4	0.68	1.82	2.08	0.82
23	May 20	14:31–15:48	≤1.5	0.8 ± 0.2	1.0 ± 0.4	0.45	1.13	0.10	0.4

[a] = calculated without NMHC
[b] = calculated including C_2–C_4 NMHC.

the aspect (b), the estimate of the uncertainty in the model predicted OH concentration. We considered following sources of error:

(1) the uncertainties in the measured concentrations of the trace gases used for model input (from Table I);
(2) the uncertainties in the input photolysis frequencies (see also Table I);
(3) the uncertainties of the reaction rate constants (from Table V).

A fourth source of model uncertainty, that of incomplete representation of the observed airmass due to missing reactions or unresolved gradients in the trace gas distribution will be subject of the discussion.

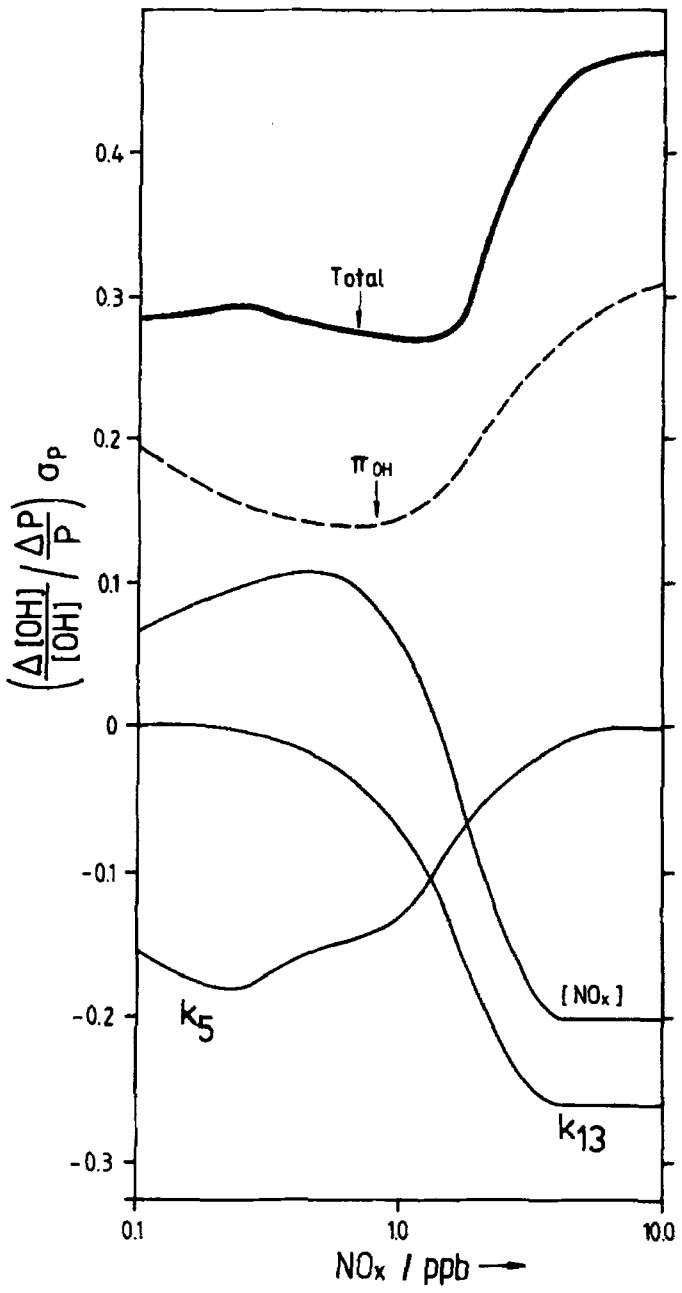

Fig. 6. The relative error of the model calculated OH concentration contributed by the relative uncertainty ΔP in various input parameters P as function of the NO_x mixing ratio. Represented are the four dominant sources of error:
error in the rate constant of reaction (5)

$$OH + CO \rightarrow H + CO_2; \qquad \sigma(k_5) = \pm 25\%,$$

error in the rate constant of reaction (13)

$$OH + NO_2 + M \rightarrow HNO_3 + M; \qquad \sigma(k_{13}) = \pm 26\%,$$

error in the measured NO_x mixing ratio $\sigma = \pm 20\%$,
error in the primary formation rate π of OH (root mean square error of J_1, k_2, k_3 and k_4) $\sigma_\pi = \pm 34\%$.
Also shown is the total error resulting from all individual uncertainties.

For the purpose of sensitivity analysis each parameter was varied individually by $\pm 10\%$ and the effect on the OH concentration was registered. As to be expected from the strongly coupled nature of the chemical system, the sensitivity of OH to a given parameter is to a certain extent also influenced by the actual values of the other parameters. This is demonstrated in Figure 6 which shows some of the calculated sensitivities as a function the NO_x mixing ratio. The mixing ratios of the other trace gases and the photolysis frequencies were fixed at the experimental values observed on May 20, 1983 (No. 21 in Table III). To represent the actual contribution to the total error in the predicted OH, the relative sensitivity of the OH-concentration to a given parameter P, namely $\Delta[OH][OH]^{-1}/\Delta P P^{-1}$, is multiplied by the relative uncertainty of that parameter, σ (as given in Tables I and V).

Figure 6 gives one example of each, the sensitivity of the predicted OH to a HO_x-production reaction, the sensitivity to a conversion reaction of OH to HO_2 and the sensitivity to an OH destruction reaction. The examples selected represent the most important members in each of these reaction families. To illustrate the dual role of NO_x – conversion of HO_2 to OH (reaction (11)) and the destruction of OH due to NO_2 (reaction (13)) – the sensitivity of the calculated OH to changes in the NO_x concentration is also included.

It is clear from Figure 6 that the sensitivity and, therefore, the error contribution of each reaction varies strongly with the NO_x concentration: thus, the error contributed by the rate constant of reaction (13) is of no consequence at low NO_x, where the net loss of OH due to reaction with NO_2 becomes unimportant. However, the same reaction provides the largest source of error among the OH loss reactions at 2 to 10 ppb of NO_x, the concentration range encountered during most of our experiments. The inverse is true for reaction (5), since at high NO_x the HO_2 produced by reaction (5) is immediately converted back to OH by reaction (11) keeping the concentration of HO_2 and, thus HO_x loss via HO_2 quite low.

Although variable, the error in the primary production π of OH via reactions (1) to (4), which is dominated by the error in the O_3 photolysis frequency, J_1, constitutes the largest single contribution at virtually all NO_x levels.

Finally we note that the sensitivity of OH to variations in the NO_x concentration itself changes sign at a NO_x mixing ratio of 1.4 ppb. This is due to the dual impact of NO_x on OH and the nonlinear dependence of the OH concentration on NO_x resulting from it. As is well known the latter curve shows a broad maximum around 1 ppb and the sensitivity curve represents its differential.

For comparison the total error of the modelled OH concentration is also included in Figure 6. It is calculated from the quadratic superposition of the relative errors from all sources and varies from 30% at low NO_x to 45% at NO_x levels of 10 ppb. We are aware that this is a crude first estimate of the total error. Moreover, strictly speaking, the total error in Figure 6 applies to the conditions on May 20, 1983. Nevertheless, a quite similar behavior is observed

for most other dates as well. This is due to the fact that the sensitivity of OH to a given parameter – although varying strongly with NO_x (see Figure 6) – depends only slightly on most of the others. Still, to account for the different NO_x, the total error of the modelled OH concentration had to be determined separately for each measurement. The resulting uncertainties are listed in Table VI along with the calculated OH concentrations for the two different treatments of NMHC. We reemphasize that the thus estimated error is based only on the uncertainties of the various input parameters namely reaction constants, photolysis frequencies and trace gas concentrations and does not include any systematic errors due – for example – to the incomplete representation of the chemical condition of the atmosphere by the model.

A comparison of the total error with the individual error contributions shows that the uncertainty in the measured photolysis rate of O_3 contributes about 40% of the total variance; clearly the accuracy of that measurement needs to be improved. But the comparison also indicates that the rate constants are still a major source of uncertainty in the predicted OH. For example, using Figure 6 to estimate the total relative error in the calculated OH for May 20, 11:31–13:05, with NO_x levels equalling 1.3 ppb, we obtain σ (OH) = ±26%. Without the error in the O_3 photolysis rate this value would only improve to σ (OH) = ±20%. Most of the remaining error is due to uncertainties in the rate constants. Clearly further improvement in the precision of the calculated OH also requires further improvement in the kinetic data.

6. Discussion

An inspection of Table VI reveals that in most cases the calcualted OH concentration exceeds the measured one by a considerable amount (see also Figures 4 and 5). This is invariably true for calculated OH concentrations above 3×10^6 cm^{-3} even for OH concentration calculated with CH_4 as the only hydrocarbon. Moreover, there seems to be a systematic trend in the sense that measured and calculated OH are mutually consistent for low calculated OH, but differ increasingly for high calculated OH. This trend becomes visible when the measured OH concentration is plotted against the calculated one. Figure 7a shows this plot for the OH calculated with CH_4 as the sole hydrocarbon, which has the advantage that it allows us to include all OH data, but this mode of calculation underestimates the OH concentration by about 20% with respect to the more complete model. Figure 7b shows the same plot for OH calculated with the more complete model including the C_2–C_4 hydrocarbons. This limits the available data to those sets for which the NMHC were measured, i.e. to 15 out of 23. Apart from shifting the calculated OH by about ±20% both figures are quite similar, and clearly show large deviations between the calculated OH concentrations above 3×10^6 cm^{-3} and the corresponding measured ones – up to a factor of 10 in the extreme case (measurement 21). Since these devia-

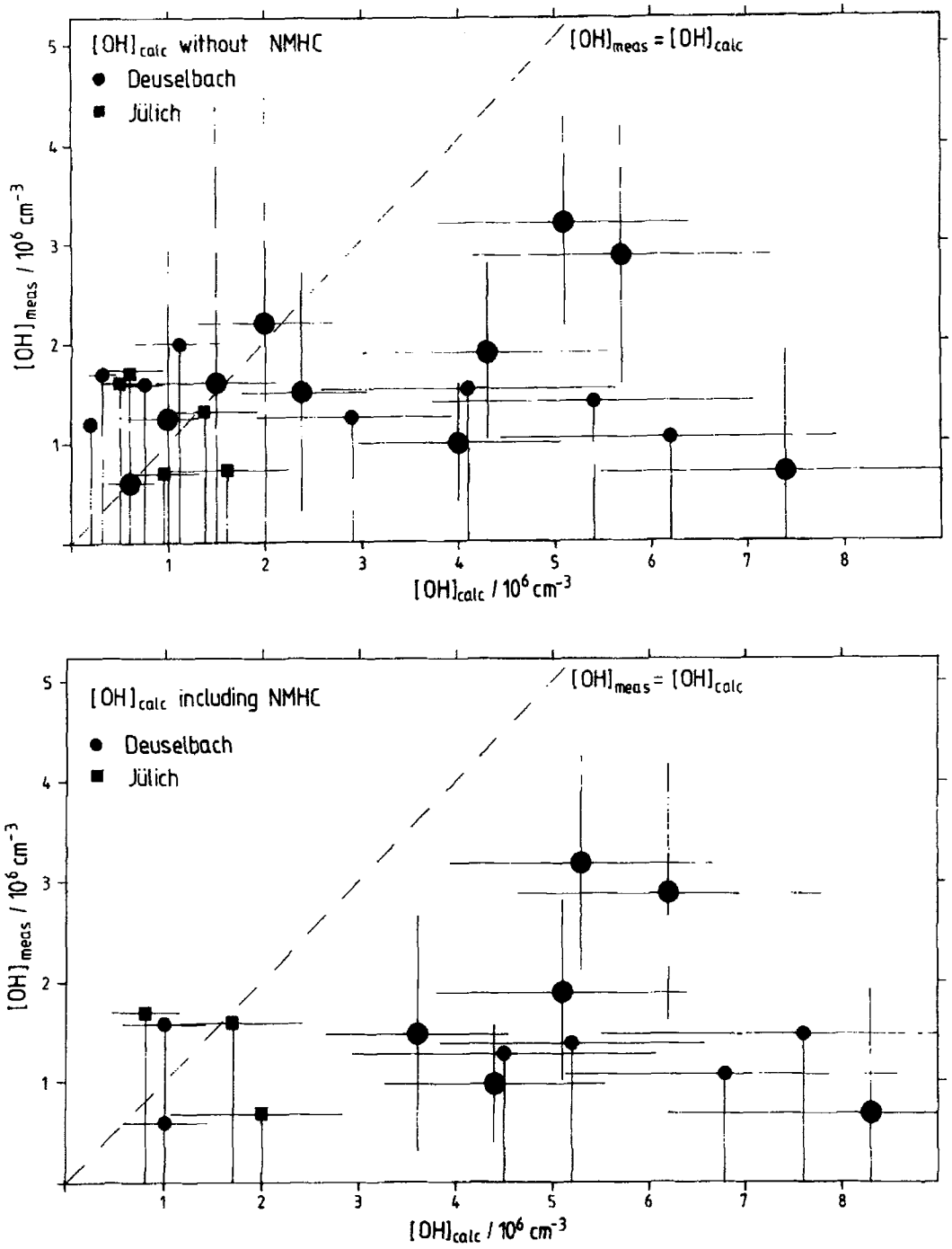

Fig. 7. Measured versus calculated OH concentration. Upper Panel a: OH calculated with CH_4 as the sole hydrocarbon. Lower Panel b: OH calculated including C_2–C_4 non methane hydrocarbons. Squares represent the values observed at Jülich, circles those at Deuselbach. Small symbols indicate upper limits.

tions are outside the estimated error limits in all cases, we believe them to be significant. However at low calculated OH concentrations ($\leqslant 2 \times 10^6$ cm^{-3}) the error bars in the measured OH concentration are so large that the conclusion of a consistency between measured and calculated OH is a weak one.

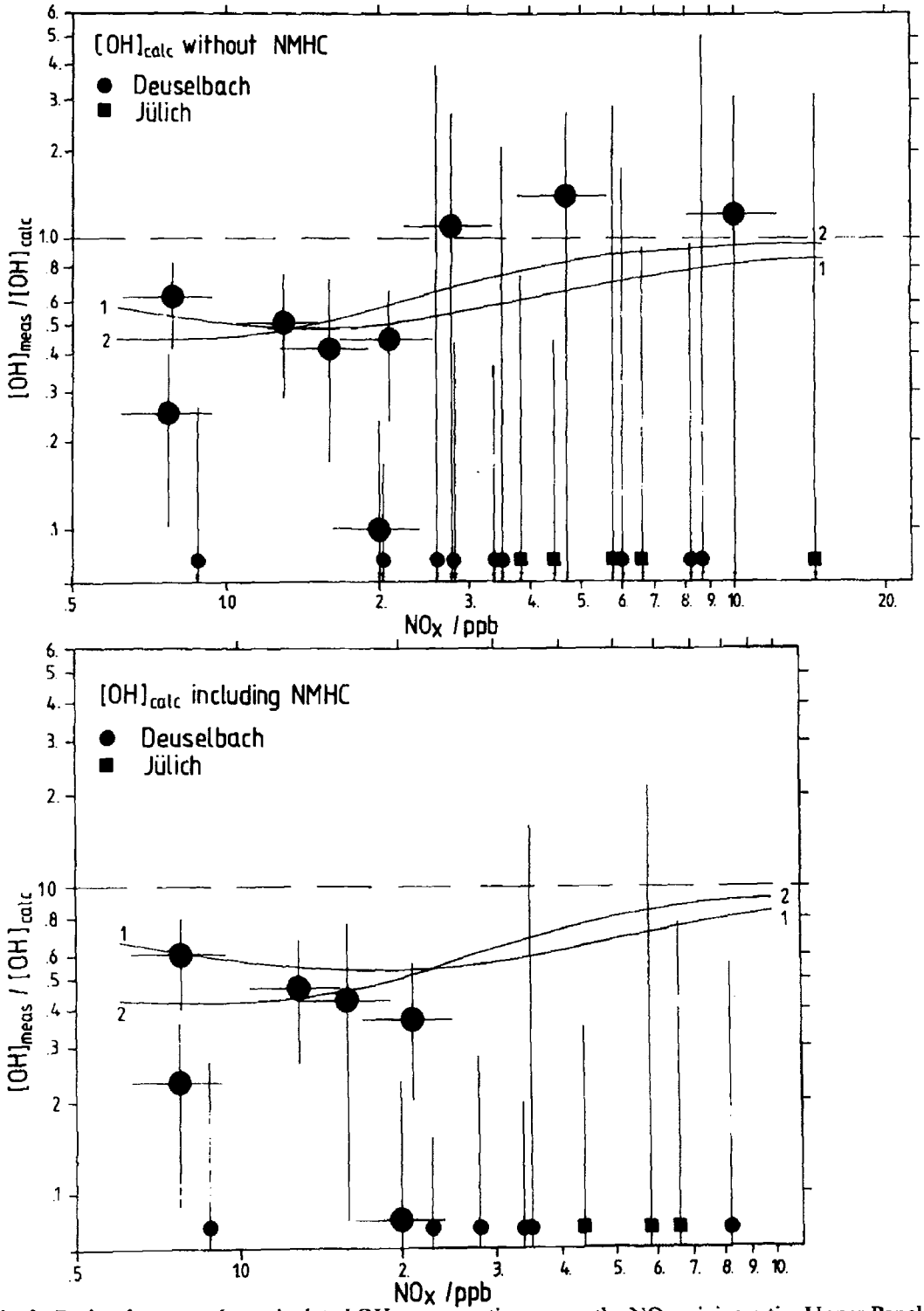

Fig. 8. Ratio of measured to calculated OH concentration versus the NO_x mixing ratio. Upper Panel a: OH calculated with CH_4 as the sole hydrocarbon. Lower Panel b: OH calculated including C_2–C_4 non methane hydrocarbons. Squares represent the measurements in Jülich, circles those at Deuselbach. The locations of measurements yielding only upper limits are identified by small symbols near the bottom of the graph, the upper ends of the vertical ines mark the 1 σ upper limits of the ratio. In those cases for clarity the error bars of NO_x are omitted. Line 1 indicates the ratio of the OH concentrations calculated with and without an additional arbitrary OH loss reaction (see text). Line 2 indicates the ratio of the OH concentrations calculated with and without an additional arbitrary loss of HO_2 and CH_3O_2 (see text).

In most situations reaction with NO_2 was the major loss process of OH and thus controlled its concentration. It is, therefore, interesting to investigate if the disagreement between calculated and measured OH varies also systematically with the NO_x concentration. Thus in Figures 8a and 8b the ratio of the measured to calculated OH concentration, R, is plotted as a function of the NO_x mixing ratio. Figure 8a, which is based on the OH calculated with CH_4 as the sole hydrocarbon, appears to exhibit a systematic trend in that ratio: At low NO_x, i.e. at high calculated OH concentrations, the ratio assumes values of about 0.5 or less, whereas at higher NO_x that ratio is closer to unity possibly reflecting better agreement between modelled and measured OH for low calculated OH concentrations. Unfortunately in the corresponding Figure 8b this trend is no longer visible, mainly since during the experiments No. 12, 13, 14 no NMHC were measured, and only upper limits but no definite values remain for the ratio of measured to modelled OH at NO_x levels above 3 ppb.

It is very interesting to note that a similar systematic trend is observed for the ratio, R_c, between measured and calculated CH_2O. It is depicted in Figure 9. For completeness the values obtained for CH_4 as sole hydrocarbon are also

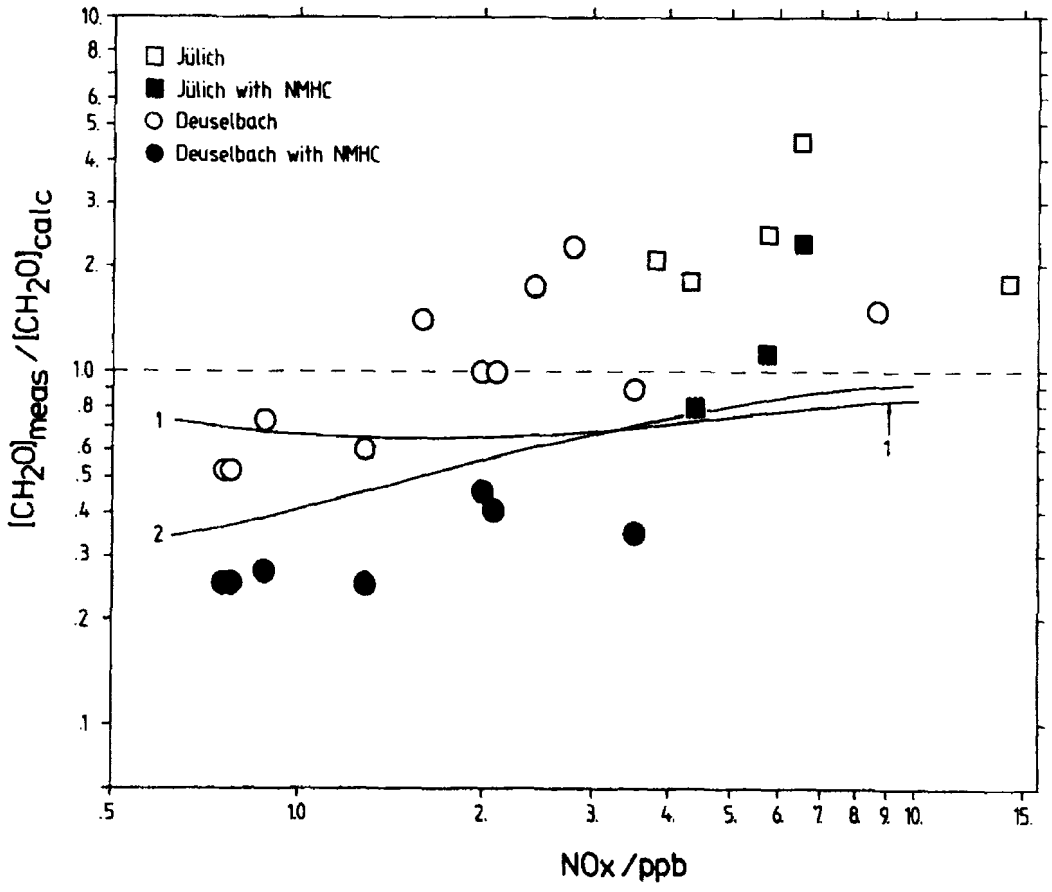

Fig. 9. Ratio of measured to calculated CH_2O versus the NO_x mixing ratio. Line 1 indicates the ratio of the CH_2O calculated with and without an additional arbitrary OH loss reaction (see text). Line 2 indicates the ratio of the CH_2O concentrations calculated with and without an additional arbitrary loss of HO_2 and CH_3O_2 (see text).

included, (although in the air masses observed most of the CH_2O must have been produced during the oxidation of nonmethane hydrocarbons.) The trend in R_c, low values at low NO_x, higher values at high NO_x, is more pronounced than that for OH. To find values of R_c larger than unity is not surprising since the hydrocarbons C_2–C_4 considered here do not encompass the full range of CH_2O producing NMHC, but it appears significant that the discrepancy between measured and calculated CH_2O reaches a factor of 0.25 for low NO_x. Below 2 ppb NO_x the model predicted CH_2O is too high even in the calculations where only CH_4 is included as the sole hydrocarbon. The lack of agreement between measured and calculated OH and CH_2O in particular at low NO_x points to a major deficiency in the model. The similar behavior of CH_2O places a constraint on the possible explanations for the model's overestimate of the OH concentration.

A priori, there is a number of possibilities to explain a difference between the measured and modelled OH concentration. The first one is that the LPA measurements provide not only a temporal but also spatial average of the OH concentration the latter of which cannot be resolved with a box model; with other words: the comparison we have made is not admissible, because a two-dimensional measurement like that by LPA can only be interpreted by a 2D model. Although this is true in principle, we believe that the error introduced by the use of a zero dimensional model is small compared to the discrepancies actually observed. We would like to illustrate this by an example. Deviations of the OH concentration along the light path from the mean are caused by changes along the path in the concentration of those trace gases, which determine the OH concentration. As was shown above, NO_x is the most important trace gas in this respect. Moreover it is the only one, whose variation causes a non-monotonic response in the OH concentration, and therefore potentially the largest deviations from the mean. To choose a worst case scenario, we assume that the average NO_x mixing ratio along the path was 1.4 ppb, made up by 0.3 ppb along the first half and 2.5 ppb along the second half of the light path. In this way the average NO_x concentration along the path would exceed that measured at the *in situ* site by nearly a factor of 5 – much more than ever observed. In that case also, the OH concentration calculated from the average NO_x mixing ratio of 1.4 ppb is right at the maximum of the OH/NO_x response curve. The OH concentrations calculated for 0.3 ppb and 2.5 ppb fall on average 30% below that maximum. Thus, even in this extreme case, we would expect the box model to overestimate a two-dimensionally calculated OH concentration by not more than 30%, a deviation which is much smaller than the differences between measured and calculated OH at low NO_x. We therefore conclude, that the observed differences are not a result of the zero-dimensionality of the model.

To explore the remaining possibilities we have to look at incomplete or erroneous representation of the atmospheric chemistry by the model. In the

following we will investigate which of the reaction types – OH production, OH/HO_2 conversion or OH destruction – could be responsible for the discrepancy between measurement and model calculation.

By far the most important reaction of the first type is the primary production of OH through O_3 photolysis (reactions (1) and (4)), and among the production reactions it alone could be responsible for a sizeable discrepancy, especially since the photolysis frequency, J_1, is one of the most uncertain input parameters. However, as Figure 6 demonstrates, the estimated contribution to the error of the calculated OH concentration from all the uncertainties in the primary OH production ranges from 15 to 32% depending on the NO_x mixing ratio. This is very much lower than the discrepancies between OH measurement and model calculation. Even with a deviation of 60% of the measured O_3-photolysis rate, J_1, from the true value, which is three times the estimated mean standard deviation (see Table I), the resulting deviation in the calculated OH would amount to only 65%. Thus, as long as there are no fundamental inconsistencies in the $O(^1D)$ reactions (2)–(4) resulting in errors of the rate constants far exceedings those given in the literature and quoted in Table V, it is safe to assume that uncertainties in the primary production of OH cannot be responsible for the large differences between measured and calculated OH.

There is another observation which points in that direction: At NO_x levels larger than 3 ppb the OH is removed nearly exclusively by a single process, the attachment of OH to NO_2 to form HNO_3, reaction (13). Then the concentration of OH is essentially determined by the ratio of the primary production and the lifetime given by reaction (13), which is relatively well determined by the experiment. Yet, in that NO_x range, calculated and measured OH values appear to agree within the error limits (Figures 7a, 7b, 8a). Although these errors are large, and the conclusion thus tentative, it still indicates that the modelled primary production of OH is essentially correct at high NO_x. This in turn argues against an uncertainty in the empirical photolysis frequencies large enough to explain the difference between calculated and measured OH at lower NO_x.

There are potentially significant secondary sources of HO_x: Photolysis of CH_2O, H_2O_2, and CH_3O_2H (reactions (21b), (19), (20), respectively). As estimated from the model calculations, however, the last two processes usually contribute far less than 10% to the total OH production. When estimated from the measured concentration, photolysis of CH_2O is also a minor source of OH. However, the model tends to overpredict the CH_2O concentration substantially, especially for low NO_x levels (see Figure 9). For those concentrations, photolysis of CH_2O can contribute up to one third of the total OH production. This overprediction of CH_2O leads to an overprediction of OH by the model. However, the effect on the calculated OH concentration is small, about 10%, because the sensitivity factor is less than 0.3. This is a consequence of the generally low sensitivity of OH to primary (see above) or secondary

production (at low NO_x-levels) and, additionally, to the reaction of CH_2O with OH (25), converting OH to HO_2. Thus, we conclude that the uncertainties in the modeling of the secondary HO_x sources neither are likely reasons for the discrepancies between calculated and measured OH.

OH–HO_2 conversion reactions too, appear to be unlikely candidates for an explanation of that difference. Even at the lowest NO_x level observed here, about a ppb, the removal of OH is still dominated by reaction (13). Moreover, within the present system of chemical reaction the conversion of OH to HO_2 and back is quite fast. The conversion of OH to HO_2 is dominated by reaction (5) with CO; HO_2 is almost exclusively converted to OH via reaction (11) with NO. Since NO was rather abundant, between 0.16 and 0.33 ppb, and the rate constant of reaction (5) is relatively fast, $k_5 = 2.4 \times 10^{-13}$ cm^3 molecules^{-1} sec^{-1}, a significant increase in the OH to HO_2 conversion rate would require the presence of one or several unknown species with a mixing ratio of the order of several ppb, even if those species reacted at nearly the collision rate. Such high concentrations are not likely at the Deuselbach station and not likely to have gone unnoticed. To decrease the calculated OH concentration by slowing down the conversion of HO_2 to OH, lower NO concentrations than those calculated from the photostationary state (reactions (26) and (32), Table V) are required. Such lower NO values have been observed and attributed to the presence of so far unidentified oxidants that convert NO to NO_2 (Parrish *et al.*, 1985). Judging from the *in situ* measurements given in Table III, however, the NO/NO_2 ratio was never far from the photostationary state, and the concentrations of that unidentified oxidant must have been small, certainly not high enough to alter the OH concentration in an appreciable way.

Thus we are left with the last class, the HO_x loss reactions, for a possible explanation of the difference between calculated and measured OH at low NO_x. To explore that possibility we introduced an arbitrary OH loss reaction in the model with a first order rate of 0.5 sec^{-1}. This changes the model predicted OH appreciably; the resulting ratio between the OH concentrations calculated with and without that loss, is plotted in Figures 8a and 8b as curve 1. Obviously it describes the data points significantly better than the straight line indicating a ratio of unity between measurement and calculation.

The introduction of this additional OH loss, however, does not improve the calculated CH_2O concentration (see curve 1, Figure 9). If we insist on this constraint, we have to argue that a process which merely removes OH is not the explanation we are looking for – at least not the full one. We therefore tried another HO_x loss mechanism: an arbitrary loss of HO_2 and – since its chemical behavior is expected to be quite similar – a simultaneous one for CH_3O_2; both with a first order rate of 0.02 sec^{-1}. The corresponding correction factors are shown as curve 2 in Figures 8a, 8b and 9. It improves the description of the OH data slightly over curve 1, and gives a considerably better representation of the CH_2O data points. We would therefore like to

suggest, that the unifying explanation for the differences between the measured and calculated values of OH and CH_2O is an additional loss of peroxyradicals unaccounted for by our model. Alternatively two or more loss mechanisms acting separately on OH, RO_2, and CH_2O are required.

The identification of mechanisms for these losses poses a more difficult problem. One suggestion has been the reaction of peroxyradicals with the surface of aerosol particles (*cf.* Warneck 1974). This certainly constitutes a sink for RO_2. But the LPA measurement of OH requires relatively good visibility, and thus the aerosol loading could not have been very high on any of the observation days. This is especially true for 1983 when the visibility was excellent and yet the highest discrepancies were found between measured and calculated OH. At that time the possible collision rate with aerosol particles must have been so small that such reactions would require a reaction efficiency of unity to be important.

Another explanation and an obvious shortcoming of our model could be the incomplete list of hydrocarbons treated. This flaw is shared with most current models. It is due to the fact that the chemistry of atmospheric hydrocarbon oxidation is complex and involves many steps which have not yet been investigated in detail. In particular the chemistry of natural hydrocarbons, e.g. isoprene or the terpenes, has not been resolved in any detail. In an attempt to model the effect of terpenes Hov *et al.* (1983) found that under certain assumptions natural hydrocarbons at the levels observed in a Norwegian pine forest may lead to a substantial decrease in the OH concentration. Since part of the area in Deuselbach is covered by conifers and the scale height of monoterpenes was shown to be comparable to the distance of the light path above ground, such an effect cannot be ruled out for our experiments. Assuming an irreversible loss of OH, 350 ppt of alpha-pinene would reduce the model predicted OH to that level observed. A more detailed and realistic reaction scheme by Lloyd *et al.* (1983) still requires 750 ppt of alpha-pinene. However, unless the products of terpene oxidation also remove CH_2O, this explanation fails to rectify the CH_2O discrepancy, since a decrease of OH alone is not sufficient for that purpose, as we just have shown. Moreover, 750 ppt of alpha-pinene is a rather high concentration to be observed outside a forest, and in the few occasions during which alpha-pinene was measured in that area, we found concentrations below 200 ppt. Isoprene, whose oxidation is known to produce copious amounts of CH_2O can, for that reason alone, be excluded as an explanation. Thus we are currently not in a position to offer a consistent mechanism for the differences between the measured and calculated values of OH and CH_2O.

7. Conclusion

The results of our OH measurements can be summarized as follows:

- Under conditions of clear-sky and low levels of anthropogenic pollution ($NO_x < 3$ ppb) the OH concentration never exceeded 3.2×10^6 cm^{-3}.
- At a more polluted site (Jülich) the upper limit was 1.7×10^6 cm^{-3}.

The model simulation including the detailed chemistry of hydrocarbons up to C_4 tends to overpredict the observed OH-concentrations by about a factor of 2 and the observed CH_2O concentrations by about a factor of 4. Considering our incomplete knowledge of NMHC oxidation mechanisms, this might be considered a relatively good agreement between measurement and calculation. However, the fact that a consistent deviation for most of the observations is obtained indicates shortcomings in the reaction scheme generally used to describe the chemistry of the tropospheric boundary layer.

All evidence points to as yet unrecognized sinks for HO_x and RO_2. In the future a more rigorous treatment of the NMHC reaction system is required. In addition measurements of the OH concentration should be made in cleaner air masses over the ocean or in the upper troposphere with much smaller concentrations of natural or man made NMHC's. A better agreement with model predicted OH might be expected under those conditions.

References

Anderson, D. E. and Meier, R. R., 1979, Effects of anisotropic multiple scattering on solar radiation in the troposphere and stratosphere, *Appl. Optics* **18**, 1955–1960.

Atkinson, R., Loyd, A. C., and Winges, L., 1982, An updated mechanism for hydrocarbon/NO_x/SO_2 photooxidation suitable for inclusion in atmospheric simulation models, *Atmos. Environ.* **16**, 1341–1355.

Campbell, M. J., Sheppard, J. C., and Au, B. F., 1979, Measurement of hydroxyl concentrations in boundary layer air by monitoring CO oxidation, *Geophys. Res. Lett.* **6**, 175–178.

Crutzen, P. J., and Gidel, L. T., 1983, A two-dimensional photochemical model of the atmosphere 2: The tropospheric budgets of the anthropogenic chlorocarbons CO, CH_4, CH_3Cl and the effect of various NO_x sources on tropospheric ozone, *J. Geophys. Res.* **88**, 6641–6661.

Davis, D. D., Heaps, W., and McGee, T., 1976, Direct measurements of natural tropospheric levels of OH via an aircraft borne tunable dye laser, *Geophys. Res. Lett.* **3**, 331–333.

Davis, D. D., Heaps, W., Philen, D., and McGee, T., 1979a, Boundary layer measurements of the OH radical in the vicinity of an isolated power plant plume: SO_2 and NO_2 chemical conversion times, *Atmos. Environ.* **13**, 1197–1203.

Davis, D. D., Heaps, W., Philen, D., Rodgers, M. O., McGee, T., and Moriarty, A. J., 1979b, Airborne laser induced fluorescence system for measuring OH and other trace gases in the parts-per-quadrillion to parts-per-trillion range, *Rev. Sci. Industr.* **50**, 1505–1516.

Davis, L. I., Guo, C., James, J. V., Morris, P. T., Postiff, R., and Wang, C. C., 1985, An airborne lidar instrument for detection of OH using the technique of laserinduced fluorescence, *J. Geophys. Res.* **90**, 12.835–12.842.

Derwent, R. G. and Eggleton, A. E. J., 1981, Two-dimensional model studies of methyl chloroform in the troposphere, *Quart. J. Roy. Met. Soc.* **107**, 231–242.

Deutscher Wetterdienst: Sonderbeobachtungen des Meteorologischen Observatoriums Hohenpeißenberg, Ergebnisse der aerologischen und bodennahen Ozonmessungen: No. 42, 1. Halbjahr 1980, 1980; No. 43, 2. Halbjahr 1980, 1981; No. 44. 1. Halbjahr 1981, 1981; No. 45, 2. Halbjahr 1981, 1982; No. 48, 2. Halbjahr 1983, 1983.

Drummond, J. W., Volz, A., and Ehhalt, D. H., 1985, An optimized chemiluminescence detector for tropospheric NO measurements, *J. Atmos. Chem.* **2**, 287–306.

Ehhalt, D. H., Rudolph, J., and Schmidt, U., 1986, On the importance of light hydrocarbons in multiphase atmospheric systems. NATO ASI Series, Vol. G6, *Chemistry of Multiphase Atmospheric Systems* (ed. W. Jaeschke), Springer-Verlag, Berlin, Heidelberg, 321–350.

Hard, T. M., O'Brien, R. J., Chan, C. Y., and Mehrabzadeh, A., 1984, Tropospheric free radical determination by FAGE, *Environ. Sci. Techn.* **18**, 768–777.

Helas, G., Flanz, M., and Warneck, P., 1981, Improved NO_x monitor for clean air regions, *Int. J. Environm. Analyt. Chem.* **10**, 155–166.

Hov, O., Schjoldager, J., and Wathne, B. M., 1983, Measurement and modelling of the concentrations of terpenes in coniferous forest air, *J. Geophys. Res.* **88**, 10.679–10.688.

Hübler, G., Perner, D., Platt, U., Tönnißen, A., and Ehhalt, D. H., 1984, Groundlevel OH radical concentration: New measurements by optical absorption, *J. Geophys. Res.* **89**, 1309–1320.

Junkermann, W., Volz, A., Platt, U., and Ehhalt, D. H., 1986, Photoelectric measurement of the solar radiation fluxes leading to the photolysis of ozone and nitrogen dioxide in the atmosphere. In preparation.

Kircher, C. C., and Sander, S. P., 1984, Kinetics and mechanism of HO_2 and DO_2 disproportionations, *J. Phys. Chem.* **88**, 2082–2091.

Levy, H., 1972, Photochemistry of the lower troposphere, *Planet. Space Sci.* **20**, 919–935.

Liu, S. C., Trainer, M., Fehsenfeld, F. C., Parrish, D. D., Williams, E. J., Fahey, D. W., Hübler, G., and Murphy, P. C., 1987, Ozone production in the rural troposphere and the implications for regional and global ozone distributions, *J. Geophys. Res.*, submitted.

Lowe, D. C., and Schmidt, U., 1983, Formaldehyde (HCHO) measurements in the non urban atmosphere, *J. Geophys. Res.* **88**, 10.844–10.858.

Lloyd, A. C., Atkinson, R., Lurmann, F. W., and Nitta, B., 1983, Modeling potential ozone impacts from natural hydrocarbons – I. Development and testing for the NO_x-air photooxidations of isoprene and α-pinene under ambient conditions, *Atmos. Environ.* **17**, 1931–1950.

NASA, 1979, *The stratosphere: Present and future*, Ref. Publ. 1049.

NASA, 1985, Chemical kinetics and photochemical data for use in stratospheric modeling, *Evaluation* No. 6, *JPL Publ.* 85–37, Sept. 15, 1985.

Parrish, D. D., Trainer, M., Williams, E. J., Fahey, D. W., Hübler, G., Eubank, C. S., Liu, S. C., Murphy, P. C., Albritton, D. L., and Fehsenfeld, F. C., 1986, Measurements of the NO_2–O_3 photostationary state at Niwot Ridge, Colorado, *J. Geophys. Res.* **91**, 5361–5370.

Perner, D., Ehhalt, D. H., Paetz, H. W., Platt, U., Röth, E. P., and Volz, A., 1976, OH-radicals in the lower troposphere, *Geophys. Res. Lett.* **3**, 466–468.

Platt, U., and Perner, D., 1983, Measurements of atmospheric trace gases by long path differential UV/visible absorption spectroscopy, *Optical and Laser Remote Sensing*, D. K. Killinger and A. Mooradian (eds.), Springer Ser. Optical Sci. **39**, 106–113.

Ridley, B. A., and Howlett, L. C., 1974, An instrument for nitric oxide measurements in the stratosphere, *Rev. Sci. Instr.* **45**, 742–746.

Rodgers, M. O., Bradshaw, J. D., Sandholm, S. T., KeSheng, S., and Davis, D. D., 1985, A 2-lambda laser-induced fluorescence field instrument for ground-based and airborne measurements of atmospheric OH, *J. Geophys. Res.* **90**, 12.819–12.834.

Rudolph, J., Ehhalt, D. H., and Gravenhorst, G., 1980, Recent measurements of light hydrocarbons in remote areas, *Proc. 1st European Symp. on the Physico-Chemical Behaviour of Atmospheric Pollutants*, Ispra, Italy, Oct. 1979.

Rudolph, J., Ehhalt, D. H., Khedim, A., and Jebsen, C., 1981, Determination of C_2–C_5 hydrocarbons in the atmosphere at low parts per 10^9 to high parts per 10^{12} levels, *J. Chrom.* **217**, 301–310.

Rumpel, K. J., 1982, *Jahresbericht des Umweltbundesamtes.*

Sheppard, I. C., Hardy, R. J., and Hopper, F., 1982, Hydroxyl radical measurements, *Antarctic J.*, 206–207.

Volz, A., Ehhalt, D. H., and Derwent, R. G., 1981, Variation of ^{14}CO and the tropospheric concentration of OH radicals, *J. Geophys. Res.* **86**, 5163–5171.

Wang, C. C., Davis, L. I., Wu, C. H., Japar, S., Niki, H., and Weinstock, B., 1975, Hydroxyl radical concentrations measured in ambient air, *Science* **189**, 797–800.

Warneck, P., 1974, On the role of OH and HO_2 radicals in the troposphere, *Tellus* **26**, 39–46.

Watanabe, T., Yoshida, M., Fujiwara, S., Abe, K., Onoe, A., Hirota, M., and Igarashi, S., 1982, Spin trapping of hydroxyl radical in the troposphere for determination by electron spin resonance and gas chromatography/mass spectrography. *Anal. Chem.* **54**, 2470–2474.

Weinstock, B., 1969, Carbon Monoxide: Residence Time in the Atmosphere. *Science* **166**, 224–225.